Towards predictive simulations of gaseous pool fires

Georgios Maragkos*, Tarek Beji, Bart Merci

Department of Flow, Heat and Combustion Mechanics, Ghent University, St. Pietersnieuwstraat 41, B-9000 Ghent, Belgium

Abstract

Focusing on advancing predictive fire modeling, large eddy simulations using improved approaches related to thermophysical, turbulence, combustion and radiation modelling are presented. More specifically, the consideration of a non-unity Lewis number, the use of the Hirschfelder-Curtiss diffusion model, the inclusion of differential diffusion and Soret effects, the application of the dynamic Smagorinsky model with a variable turbulent Prandtl number, an eddy dissipation concept model with dynamically determined coefficients for combustion and the weighted-sum-of-gray-gases model for radiation have been included in a modified version of fireFoam 2.2.x. A comprehensive comparison between the predictions of the modified code against the standard version of fireFoam and experimental data of a medium-scale 24.6 kW methanol pool fire is presented. Evaporation modelling is not yet included.

Keywords: LES, diffusion, dynamic Smagorinsky, EDC, WSGGM

*Corresponding author:
Email address: Georgios.Maragkos@UGent.be (Georgios Maragkos)

1. Introduction

Progress in fire safety science and engineering, nowadays more than ever, relies on the use of Computation Fluid Dynamics (CFD) for simulating fire scenarios that would either be too expensive to conduct experimentally or too complex to analyze by using analytical solutions or two-zone model approaches. With the ever increasing capabilities of computer hardware and improvements in software, the use of CFD has become a valuable tool in the hands of fire safety engineers working on modelling real-life fire scenarios (e.g., fire detection, fire suppression, design of smoke control systems) [1]. The use of Large Eddy Simulations (LES) has become increasingly popular in both academia and industry. Fire-related CFD codes now have the possibility to employ high performance computing with sufficiently high grid resolutions using more advanced modelling approaches. Within this context, accurate and reliable modelling of the physics, considering all the different physical processes occurring in fire scenarios, is crucial.

The main goal of the paper, focusing on advancing predictive fire modeling, is to report on LES using improved approaches related to thermophysical, turbulence, combustion and radiation modelling and to evaluate how well these models perform against some of the standard models often employed for numerical simulations of fire scenarios. The present work extends our previous study [2] and aims to demonstrate how incorporation of these modelling approaches in a fire-related CFD code enhances its predictive capabilities. We focus on the gas phase. While the processes in the solid and/or liquid phase are also very important, the present study avoids modelling uncertainties there. Moreover, the gas phase is also crucial since

reliable fire simulations always strongly rely on accurate predictions of the flame rise temperatures, heat fluxes and the flow field. The experimental case used for validation purposes here is the medium-scale, 30.5 cm in diameter, 24.6 kW methanol pool fire experiments [3], one of the target cases of the newly established MaCFP workshop series [4] that aims to make systematic progress in fire modelling.

2. Models

A modified version of fireFoam 2.2.x [5], originally developed by FM Global, is employed here. The code uses a fully compressible flow formulation and solves the Navier-Stokes equations, along with transport equations for species mass fractions and sensible enthalpy, using Favre-filtered quantities. A non-unity Lewis number is employed along with the use of the Hirschfelder-Curtiss diffusion model and the inclusion of differential diffusion and Soret effects. A detailed presentation of the code has been reported [2], so only a general overview is outlined here. Recent developments in combustion and radiation modelling are presented in detail.

The dynamic Smagorinsky model [6] is used, calculating the sub-grid scale viscosity as:

$$\mu_{sgs} = \overline{\rho}(c_s\Delta)^2|\widetilde{S}| \tag{1}$$

where Δ is the filter width (taken as the cube root of the cell volume) and S is the strain rate. The dynamic procedure employed for determining $(c_s\Delta)^2$ does not allow for negative values while no upper bound is defined.

The sub-grid kinetic energy is estimated as:

$$k_{sgs} = c_I\Delta^2|\widetilde{S}|^2 \tag{2}$$

with the model parameter c_I computed dynamically as $c_I = \langle L_{kk} M_{kk} \rangle / \langle M_{kk} M_{kk} \rangle$ where the brackets denote averages, computed as local averages of their face values, with $L_{kk} = \widehat{\overline{\rho}\widetilde{u}_k\widetilde{u}_k} - \widehat{\overline{\rho}\widetilde{u}_k}\widehat{\overline{\rho}\widetilde{u}_k}/\widehat{\overline{\rho}}$ and $M_{kk} = 2\widehat{\Delta}^2\widehat{\overline{\rho}}|\breve{\widetilde{S}}|^2 - 2\widehat{\Delta^2\overline{\rho}|\widetilde{S}|^2}$ (where $\breve{\widetilde{f}} = \widehat{\overline{\rho f}}/\widehat{\overline{\rho}}$). The calculation of c_I differs from [2]: it is made consistent with the Smagorinsky model since the dynamically determined coefficients are now both squared.

The sub-grid scale dissipation rate is modelled as:

$$\epsilon_{sgs} = \frac{c_\epsilon k_{sgs}^{3/2}}{\Delta} \tag{3}$$

where $c_\epsilon = 1.0$ [2] is a model constant.

The sub-grid scale thermal diffusivity is calculated as $\alpha_{sgs} = \mu_{sgs}/Pr_t$ with the turbulent Prandtl number, Pr_t, determined from a dynamic procedure [2]. The Pr_t values are clipped between 0.01 and 1.0 for numerical stability. Finally, it is assumed that $Sc_t = Pr_t$.

Combustion is modelled through the Eddy Dissipation Concept (EDC) [7]. The version presented below is based on [8]. According to the energy cascade theory, the largest energy-containing eddies are highly unstable and break down into smaller eddies until they are sufficiently small (i.e., have the size of the Kolmogorov length scale) and they are dissipated into heat. Within EDC, these small eddies are called fine structures and such regions can be treated as, e.g., Perfectly Stirred Reactors (PSR) in which chemical reactions depend on the molecular mixing between the reactants. These fine structures are intermittently distributed and only a fraction of them can react. By considering a one-step, infinitely fast, irreversible chemical

reaction, the fuel reaction rate is calculated as:

$$\overline{\dot{\omega}_F'''} = \overline{\rho}\frac{\gamma^2\chi}{\tau(1-\gamma^3\chi)}min\left(\widetilde{Y}_F, \frac{\widetilde{Y}_{O_2}}{s}\right) \tag{4}$$

where γ is the size of the fine structures, τ is the mixing time scale, χ is the reactive part of the fine structures, s is the oxygen-fuel mass stoichiometric ratio while $\widetilde{Y}_F$ and $\widetilde{Y}_{O_2}$ are the filtered mass fractions of fuel and oxygen, respectively.

The size of the fine structures can be expressed as:

$$\gamma = C_\gamma\left(\frac{\nu\epsilon_{sgs}}{k_{sgs}^2}\right)^{1/4} \tag{5}$$

with $\gamma < 1$ and C_γ a model parameter calculated as [8]:

$$C_\gamma = Da_\eta^{1/2}(Re_T + 1)^{1/2} \tag{6}$$

with Da_η the Damköhler number, evaluated at the Kolmogorov scale, and Re_T the turbulent Reynolds number.

For infinitely fast chemistry, χ is calculated as [9]:

$$\chi = \begin{cases} \frac{s\widetilde{Y}_{ref}+Y_{O_2}^0}{Y_{O_2}^0}, & \text{if } \widetilde{Y}_{ref} < 0 \\ \frac{Y_F^0-\widetilde{Y}_{ref}}{Y_F^0}, & \text{if } \widetilde{Y}_{ref} \geq 0 \end{cases} \tag{7}$$

where Y_F^0 is the initial fuel mass fraction in the fuel stream, $Y_{O_2}^0$ is the initial oxygen mass fraction in the oxidizer stream and $\widetilde{Y}_{ref} = \widetilde{Y}_F - \widetilde{Y}_{O_2}/s$.

The estimation of the mixing time scale is modified compared to the original formulation of the model as:

$$\tau = min(\tau_{turb}, \tau_{lam}); \tag{8}$$

which effectively considers mixing under turbulent and laminar conditions. The turbulent time scale is based on the original energy cascade model by Ertesvåg and Magnussen [10], taken as the Kolmogorov time scale:

$$\tau_{turb} = C_\tau \left(\frac{\nu}{\epsilon_{sgs}} \right)^{0.5} \tag{9}$$

where C_τ is a model parameter calculated as [8]:

$$C_\tau = \frac{1}{Da_\eta (Re_T + 1)} \tag{10}$$

while the laminar time scale is estimated as:

$$\tau_{lam} = \frac{\Delta^2}{C_{diff} \nu} \tag{11}$$

where $C_{diff} = 4$ is a model constant.

The Damköhler number, comparing the molecular mixing process at the Kolmogorov scale to the reaction in the fine structures, is evaluated as $Da_\eta = \tau_\eta / \tau_c$ where $\tau_\eta = (\nu / \epsilon_{sgs})^{0.5}$ is the Kolmogorov time scale. The characteristic chemical time scale is evaluated by considering an Arrhenius equation as $\tau_c = A e^{-T_A/T}$ where $A = 1.79949 \times 10^{10}$ s^{-1} is the pre-exponential factor and $T_A = 15095.7$ K is the activation temperature for a global one-step methanol reaction [11].

The turbulent Reynolds number is calculated based on the sub-grid scale kinetic energy and dissipation rate as $Re_T = k_{sgs}^2 / (\nu \epsilon_{sgs})$. In regions where Re_T becomes low (i.e., laminar conditions), the calculation of the fuel reaction rate can become problematic: it can increase drastically and can potentially lead to unphysical behavior [12]. To prevent this problem, the ratio $(\gamma^2 \chi)/(1 - \gamma^3 \chi)$ is clipped to values ≤ 1 [12]. It has also been reported (e.g.,

[12]) that the coefficients C_γ and C_τ often need to be calibrated for different scenarios. Here, the dynamic determination of the coefficients is an important extension of the model, compared to [2], where constant coefficients where used.

For radiation modelling, the radiative intensity is treated as a function of both spatial location and angular direction and is obtained by solving the radiative transfer equation (RTE) by the finite volume discrete ordinates model (fvDOM). The absorption/emission is modelled through the weighted-sum-of-gray-gases model (WSGGM). Within WSGGM, the total emissivity and absorptivity (assuming $\alpha = \epsilon$) of a gas mixture is calculated as the sum of fictitious gray gases weighted with a temperature dependent weighting factor as:

$$\widetilde{\epsilon} = \sum_{i=0}^{I} \widetilde{a}_{\epsilon,i}(T)\left(1 - e^{-\kappa_i p L}\right) \tag{12}$$

where $a_{\epsilon,i}$ is the emissivity weight factor of the i fictitious gray gas, κ_i is the absorption coefficient of the i gray gas, p is the sum of the partial pressures of all absorbing gases and L is the path length, calculated as $L = 3.6V/A$. The volume, V, is calculated by summing all the cell volumes where reaction takes place. Assuming a conical shape, then the corresponding surface area, A, can be calculated. This approach bypasses any modelling uncertainties related to prescribing a fixed path length and allows it to vary dynamically during the numerical simulations. The temperature dependence of $a_{\epsilon,i}$ is calculated as:

$$\widetilde{a}_{\epsilon,i} = \sum_{i=0}^{J} b_{\epsilon,i,j} \widetilde{T}^{j-1} \tag{13}$$

where $b_{\epsilon,i,j}$ are the emissivity gas temperature polynomial coefficients. The coefficients $b_{\epsilon,i,j}$ and κ_i are taken from [13]. The total absorptivity is then

calculated as:

$$\widetilde{a} = -\frac{ln(1-\widetilde{\epsilon})}{L} \tag{14}$$

and the radiative heat fluxes are calculated as:

$$\nabla \cdot \overline{\dot{q}_r''} = \widetilde{a}(4\sigma\widetilde{T}^4 - \widetilde{G}) \tag{15}$$

where σ is the Stefan-Boltzmann constant and G is the total irradiance. Turbulence-chemistry interaction (TRI) is neglected at present. The current approach aims to accurately predict the radiative fraction in the numerical simulations, as opposed to prescribing it. This is another significant step forward compared to [2].

Comparisons are made with the standard version of fireFoam 2.2.x. The code assumes equal species diffusivities and unity Lewis number. Fick's law is used for diffusion and the Soret effect is neglected. The constant Smagorinsky model is applied for turbulence, with $c_s = 0.1$. For combustion, the Eddy Dissipation Model (EDM) is available, calculating the fuel reaction rate as $\overline{\dot{\omega}_F'''} = \overline{\rho}\frac{min(\widetilde{Y}_F, \widetilde{Y}_{O_2}/s)}{\tau_{mix}}$ where $\tau_{mix} = min\left(\frac{k_{sgs}}{C_{EDM}\epsilon_{sgs}}, \frac{\Delta^2}{C_{diff}\alpha}\right)$ with $C_{EDM} = 4$, $C_{diff} = 4$. For radiation the fvDOM model is applied. Under the assumption of a non-absorbing, optically thin medium, the radiative heat fluxes are calculated as $\nabla \cdot \overline{\dot{q}_r''} = \chi_r \overline{\dot{q}_c'''}$ where $\chi_r = 0.18$ [14] is a constant radiative fraction for methanol and $\overline{\dot{q}_c'''}$ is the local heat release rate per unit volume. In general, the choice of these specific models in fireFoam is very common for fire simulations.

3. Numerical setup

A cylindrical domain of 1.5 m x 1.8 m is used for the simulations. The mesh consists of almost uniform cells on the centerline and at the base of the

fuel inlet, while it is stretched towards the sides and top of the domain. A refinement region, covering the full fire plume area, of 0.6 m in diameter and 0.9 m in height is used having grid sizes of approximately 0.5 cm. This grid size was chosen based on a grid sensitivity study shown later in Figure 3. A 1 cm high wall surrounding the fuel inlet, having one cell thickness, represents the 1 cm rim reported in the experiments [3]. The inclusion of the rim, not considered in [2], is important in order to accurately capture the unsteady behavior of the methanol pool fire. The resulting number of cells across the fuel inlet is 60 while the total number of cells is approximately 985000.

In the absence of an evaporation model, and avoiding related modelling uncertainties, the liquid methanol is modelled directly as gaseous species, considered to be fully evaporated right above the fuel surface. The mass flow rate is applied at the inlet (accounting for both convective and diffusive mass fluxes), calculated based on the experimentally reported methanol feeding rate of 1.35 cm^3/s and a liquid fuel density of 792 kg/m^3. The resulting heat release rate is approximately 22.6 kW. The temperature at the inlet is set to 338 K, corresponding to the boiling point of methanol, while the ambient temperature and pressure are 293 K and 101325 Pa, respectively. For the solution of the RTE, 72 solid angles are used for angular discretization. A variable time step with a maximum Courant number of 0.9 is employed.

4. Results

A comparison between the simulations and the experiments is presented here. An experimental uncertainty of 5% was reported for the mean and rms values of velocity and mean values of temperature while 30% errors were esti-

mated for the rms temperatures. Results with the new and standard models of fireFoam are here referred to as 'New' and 'Old', respectively. The simulations were run for 65 s, averaging over the last 60 s (i.e., about 100 flows through time) to produce time-averaged quantities. The total physical running time for the 'New' and 'Old' case was 101.2 h and 70.8 h, respectively, on a Dell PowerEdge R630 server with 2x12-core Intel Xeon E5-2680v3, 2.5GHz and 128GB RAM.

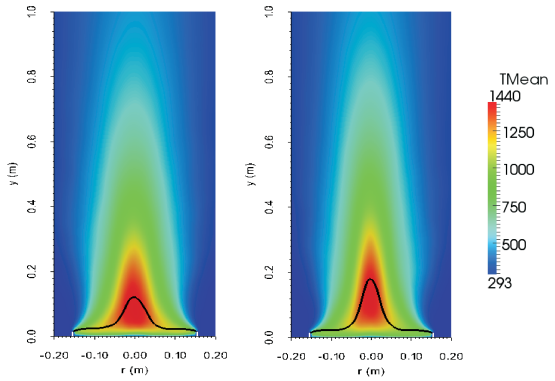

(a) (b)

Figure 1: 2D plots of mean temperature for (a) New and (b) Old case. Maximum flame temperatures: $T_{max,\ New} = 1440$ K and $T_{max,\ Old} = 1436$ K. Solid black line: stoichiometric mixture fraction of 0.1346.

A qualitative comparison between the two cases is given in Figure 1, presenting 2D contour plots of the predicted mean temperature distribution. Overall, similar flame structures are obtained with comparable maximum flame temperatures ($\approx$ 1440 K). However, the 'Old' case exhibits higher temperature regions on the centerline at higher locations. Given the fact that no correction was made for the effects of radiation on the experimental data of temperature (in the order of 5%) [3], the maximum flame tempera-

tures obtained for both cases are considered to be in good agreement with the experiments (i.e., 1330 K [3]). Such a correction has been applied to the numerical results for temperature presented later. However, clear differences are observed at the location of the stoichiometric mixture fraction. This implies differences in the predicted species distributions. It is interesting to note that values of stoichiometric mixture fraction are found at the sides right above the burner rim, implying that reaction takes place there and flames are attached. This was verified by examining instantaneous plots of temperature during the simulations and was also reported in the experiments [3]. Numerical simulations without the rim (not shown here), as in [2], revealed that not only the temperature profiles become narrower but also resulted in the fire plume to break further downstream influencing the centerline temperature distribution. Finally, it is noted that the shape of the stoichiometric mixture fraction contour, with an important horizontal region from the sides towards the center, very close to the fuel surface, indicates it is important to accurately simulate this region. This is particularly true if evaporation is to be simulated. In that case, the boundary layer flow must be resolved, which can impose additional grid requirements.

Table 1: Comparison of flame height, radiative fraction and puffing frequency between simulations and experiments. New: χ_r predicted, Old: χ_r prescribed.

Case	L_f (cm)	χ_r (-)	f (Hz)
Exp.	50.8 [14]	0.18-0.2 [14, 15]	2.8 [3]
New	46.7	0.197	2.77
Old	50.1	[0.18]	2.71

A more quantitative comparison is presented in Table 1, reporting several characteristic parameters related to the pool fire dynamics. The predicted mean flame height is defined as the axial location where the integrated heat release rate is 99% of the total heat release rate. The radiative fraction is calculated as the ratio of the integrated radiative heat fluxes on all the domain boundaries over the integrated heat release rate inside the domain. The puffing frequency has been obtained from a fast Fourier transform analysis of the axial velocity on the centerline at $y = 0.2$ m. The predicted flame heights and puffing frequencies for both cases are in very good agreement with the experimental data, although, the criterion used to determine the flame height experimentally is different (based on a 50% flame intermittency). It is interesting to look at the predictions of the radiative fractions for both cases. The 18% radiative fraction for the 'Old' case is expected since it was prescribed. On the other hand, the 'New' case predicts a radiative fraction of 19.7% which is in excellent agreement with the reported values in literature. The fact that the 'New' case is able to accurately predict the radiative fraction is an important step forward towards predictive fire modelling. This is not straightforward (e.g., the application of the grey gas model might require the use of a calibration factor to artificially reduce the absorption coefficient and obtain better prediction of the radiative fraction [16]). In other words, while the differences between the 'New' and 'Old' may seem minor at first sight in Table 1, an essential difference is that the 'New' results do not involve tuning of any kind and are thus 'predictive'. We now focus in more detail on profiles.

The differences in the combustion (e.g., calculation of the fuel reaction

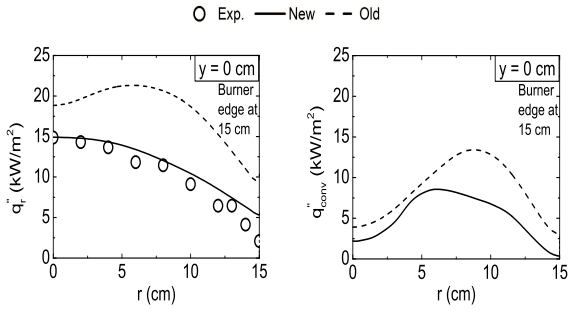

(a) (b)

Figure 2: Distribution of (a) radiative and (b) convective heat fluxes at the pool surface. Experimental data taken from [17].

rate) and radiation (e.g., neglect of absorption and assumption of constant local emission based on a prescribed χ_r) modelling have a direct impact in the predictions of the radiative heat fluxes at the pool surface shown in Figure 2(a). The 'New' predictions are in excellent agreement with the experiments, while the 'Old' results severely over-predict the radiative heat fluxes with discrepancies up to 75%. Similar differences between the two cases are observed for the convective heat fluxes (Figure 2(b)). Even though on the same order of magnitude, the radiative heat fluxes play a more important role in the heat feedback to the fuel surface compared to the convective heat fluxes which is in line with [15]. Good agreement for the heat fluxes is essential when modelling the liquid evaporation.

The axial distribution for the mean and rms temperatures and axial velocities is presented in Figure 3. In general, better predictions are obtained for the 'New' case which are in good agreement with the experimental data, particularly the predictions for the mean and rms temperatures. This is very important with respect to heat transfer in fire simulations. The rms temper-

atures on the centerline are slightly under-predicted close to the fuel source for the 'Old' case. It is postulated that the inclusion of an evaporation model would increase the rms temperatures in the near field region of the methanol pool fire due to the fluctuating thermal feedback on the fuel surface. Similar trends are observed for the mean and rms axial velocities for both cases.

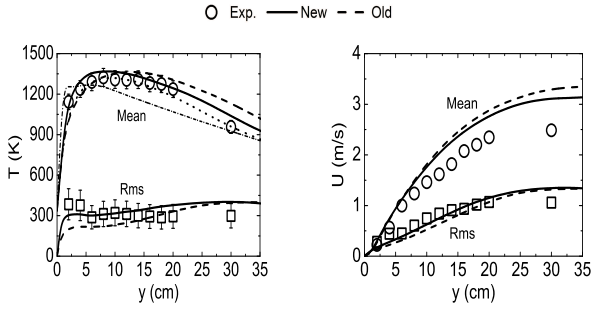

Figure 3: Axial distribution of centerline mean and rms (a) temperatures and (b) axial velocities. Dot: New-1 cm, Dash-dot: New-2 cm.

The radial distribution of the mean and rms temperatures at different heights above the pool fire is presented in Figure 4. The wider temperature profiles for the 'New' case at $y = 6$ cm could be attributed to the improved thermophysical modelling since laminar diffusion effects were reported up to a height of $y = 10$ cm [3]. The lower mean values with the 'New' case on the centerline at location $y = 30$ cm clearly agree much better with the experimental data (over-predictions of 8.5% vs 18.3% for the 'New' and 'Old' cases, respectively). While slightly over-predicted on the centerline at $y = 30$ cm, the rms temperatures remain within the experimental uncertainty everywhere else examined.

The radial distribution of the mean and rms axial velocities (Figure 5) follows the same pattern. The buoyancy-induced increase of the centerline

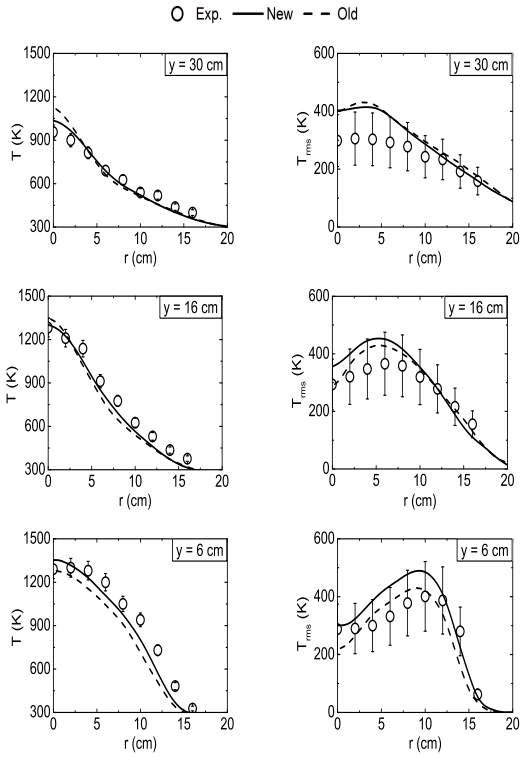

Figure 4: Radial distribution of (a) mean and (b) rms temperatures at various heights.

axial velocity is too strong, leading to a 24% and 32% over-estimation for the 'New' and 'Old' cases, respectively, at $y = 30$ cm, due to the over-predicted temperatures.

Figure 6 presents the radial distribution of the mean and rms radial velocities. The characteristic puffing behavior of pool fires results in high radial velocities close to the fuel surface, entraining air towards the reaction zone. Accurate prediction of the entrainment is important since it affects not only the radial distribution of the flame temperatures but also the centerline temperatures and the resulting puffing frequency. In general, the

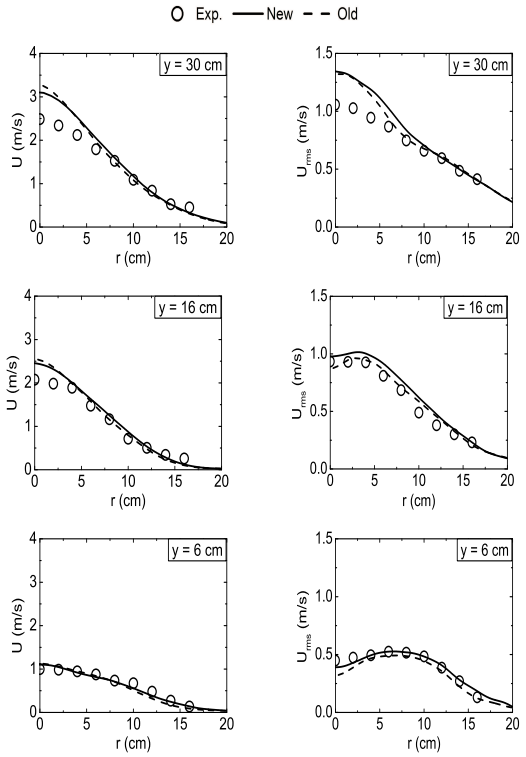

Figure 5: Radial distribution of (a) mean and (b) rms axial velocities at various heights.

agreement for both cases with the experiments is reasonable. An overall 20% over-prediction of the mean radial velocities is observed close to the pool surface ($y = 6$ cm) but they remain fairly well predicted further downstream. Reasonable agreement for the rms radial velocities is observed, although the experimental values are under-predicted at all locations examined. The over-predicted mean radial velocities close to the pool fire surface ($y = 6$ cm) explain the slightly narrower temperature profiles at the same location.

For completeness, the axial distributions of the main chemical species from the simulations are compared with the experimental data (having 24%

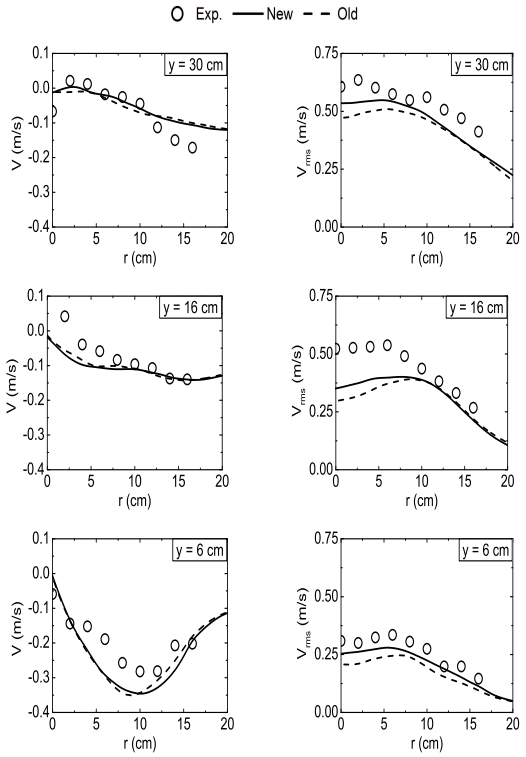

Figure 6: Radial distribution of (a) mean and (b) rms radial velocities at various heights.

uncertainty) reported in [17]. The 'New' results are considered to be, overall, better than'Old' mainly due to the lower CO_2 predictions. The differences in the axial locations where stoichiometric mixture fraction exists between the two cases (Figure 1) are here confirmed from the axial distribution of CH_3OH. It is obvious that the use of a single-step reaction is not sufficient to accurately capture the production of CO_2 and H_2O concentrations. The use of finite rate chemistry, by considering CO and H_2, would greatly improve the present predictions.

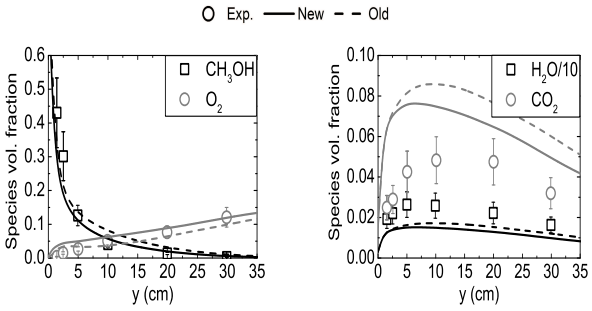

(a) (b)

Figure 7: Axial distribution of (a) CH_3OH, O_2 and (b) H_2O, CO_2. Experimental data taken from [17].

5. Conclusions

Improved modelling approaches related to thermophysical, turbulence, combustion and radiation were presented for LES with a modified version of fireFoam 2.2.x. The 'New' predictions were compared against some of the usual modelling approaches in the fire community using the standard version of fireFoam and with medium-scale methanol pool fires [3]. In general, the 'New' predictions, with models having dynamically determined coefficients, had the significant advantage that their model parameters can vary depending on the local properties of the flow and no calibration is needed. In other words: they are truly predictive.

Overall, the 'New' and 'Old' predictions were comparable for some characteristic parameters of pool fires (i.e., flame height and puffing frequency). These predictions were also in very good agreement with the experimental data. However, clear improvements were observed in the 'New' predicted centerline temperatures and in the radiative heat fluxes at the pool surface (the 'Old' results significantly over-predicting the experimental values by up

to 18.3% and 75%, respectively). Differences in rms temperatures, as well as in the flow field, were smaller. The 'New' centerline predictions for CO_2 concentrations were closer to the experiments. Finally, the 'New' predictions with the use of the WSGGM model for radiation accurately predicted the experimentally reported radiative fraction of the methanol pool fire.

Acknowledgments

Funded by Ghent University (Belgium) through GOA project BOF16/GOA/004.

References

[1] B. Merci, Fire Safety Science 11 (2014) 46-65.

[2] G. Maragkos, T. Beji, B. Merci, Combust. Flame 181 (2017) 22-38.

[3] E.J. Weckman, A.B. Strong, Combust. Flame 105 (1996) 245-266.

[4] https://github.com/MaCFP

[5] https://github.com/fireFoam-dev

[6] P. Moin, K. Squires, W.H. Cabot, S. Lee, Phys. Fluids A 3 (1991) 2746-2757.

[7] B.F. Magnussen, 19^{th} AIAA Aerospace Science Meeting, 1981.

[8] A. Parente, M.R. Malik, F. Contino, B.B. Dally, Fuel 163 (2016) 98-111.

[9] Z. Chen, J. Wen, B. Xu, S. Dembele, Int. J. Heat Mass Transf. 70 (2014) 389-408.

[10] I.S. Ertesvåg, B.F. Magnussen, Combust. Sci. Technol. 159 (2000) 213-235.

[11] C.K. Westbrook, F.L. Dryer, Combust. Sci. Technol. 27 (1981) 31-43.

[12] A. De, E. Oldenhof, P. Sathiah, D. Roekaerts, Flow Turbul. Combust. 87 (2011) 537-567.

[13] L.J. Dorigon, G. Duciak, R. Brittes, F. Cassol, M. Galarca, F.H.R. Franca, Int. J. Heat Mass Transf. 64 (2013) 863-873.

[14] M. Klassen, J. Gore, Structure and Radiation Properties of Pool Fires, NIST-GCR-94-651, 1992.

[15] A. Hamins, S.J. Fischer, T. Kashiwagi, M.E. Klassen, J.P. Gore, Combust. Sci. Technol. 97 (1993) 37-62.

[16] J.L. Rhatigan, H. Bedir, J.S. T'ien, Combust. Flame, 112 (1998) 231-241.

[17] A. Hamins, A. Lock, The Structure of a Moderate-Scale Methanol Pool Fire, NIST Technical note 1928, 2016.